Ultra-fast precipitation of transient amorphous cerium oxalate in concentrated nitric acid media

DOI: 10 1039/x0xx00000x

Isaac Rodríguez-Ruiz,[a]* Sophie Charton,[a]* Dimitri Radajewski,[b] Thomas Bizien [c] and Sébastien Teychené [b]

Amorphous cerium oxalate precipitation is here characterized and reported for the first time as a primary nucleating transient precursor for a more stable crystalline hydrated phase, at high supersaturations and in strong acid solutions. Preliminary results point out an initial binodal phase separation leading to precipitation.

Introduction

Rare earths precipitation using oxalic acid is common in hydrometallurgical recycling processes, such as in the recycling of permanent magnets, lamp phosphors and LED light sources, rechargeable batteries or catalysts.[1] Oxalic precipitation is also a major step in the irradiated nuclear fuel reprocessing industry, where plutonium is recovered from highly concentrated nitric acid solutions, in the range of 1-7 mol L^{-1}, by reactive crystallization with oxalic acid.[2] In this framework, cerium and neodymium, which display close thermodynamic properties as plutonium in solution, are widely used as models for R&D purposes, thus avoiding tedious manipulation of radioactive species.

As in most crystallisation processes, a strong challenge in fast precipitation is to control the solid phase formation kinetics, since the size and morphology of the precipitated particles greatly influence their properties and/or the subsequent steps of the process (filtration, etc.). Significant efforts have been made so far in order to address mixing and transport issues.[3, 4] However, the major and key parameter affecting the final shape and the size of the particles is the rate of crystal formation, *i.e.* the nucleation rate. In this regard, a thorough comprehension of the mechanisms involved in the process is needed.

The precipitation reaction of cerium nitrate in oxalic acid media leads to the formation of $Ce_2(C_2O_4)_3{\cdot}10H_2O$, a white solid,[5] in accordance with the overall balance equation:

$$2Ce(NO_3)_3 + 3C_2H_2O_4 + 10H_2O \rightarrow Ce_2(C_2O_4)_3{\cdot}10H_2O + 6HNO_3 \quad (1)$$

Very little has been investigated so far regarding the out-of-equilibrium evolution of this system during the initial stages of reaction, and the understanding of the mechanisms involved in cerium oxalate (CeOX) precipitation/nucleation are still poorly understood. With a view to shed some light into these problematics, CeOX precipitation experiments have been performed at room temperature in small volumes using two different experimental setups. First, a series of microscopy observations over microliter sized batch reactions were carried out, allowing to observe the reaction in a time scale from 1 second to few minutes after precipitation. Second, to monitor the first instants of the fast precipitation reaction (below 1 second reaction time), small angle X-ray scattering (SAXS) preliminary experiments performed in an original microfluidic setup are presented. In both experimental setups, due to the stochastic nature of nucleation[6] the study of small volumes enables the location of the nucleation events in space, facilitating their observation and characterization.[7, 8]

Experimental

Reagents and solutions preparation

$Ce(NO_3)_3$ (99.9%), $C_2H_2O_4$ (99%) and HNO_3 (70%) ACS reagents were used to prepare two mother solutions using deionized water (DIW), with the following concentrations, given in molality units (m): A) $Ce(NO_3)_3$ 0.1 m+ HNO_3 1 m; and B) $H_2C_2O_4$ 0.15 m. Dilutions of the mother solutions were prepared respectively using a HNO_3 1 m solution and DIW. All solutions were filtered using a Millipore 0.2 µm pore filter prior to their use. Experiments were performed by mixing $Ce(NO_3)_3$ solutions of different concentrations, ranging from 0.05 m to 0.1 m, to the corresponding stoichiometric solutions of oxalic acid.

Microscopy observations

[a] CEA, DEN, Research Department on Mining and Fuel Reprocessing Processes, SA2I, F-30207, Bagnols-sur-Cèze, France. Email: isaac.rodriguez@cea.fr; sophie.charton@cea.fr
[b] Laboratoire de Génie Chimique, Université de Toulouse CNRS, INPT, UPS, UMR 5503, 4 allée Emile Monso, Toulouse, France
[c] SWING beamline, Synchrotron Soleil, Gif-sur-Yvette, France

For optical microscopy (OM) observations, 1 µL droplets of solutions A and B were deposited on top of a hydrophobized glass slide. Subsequently, droplets were flattened by covering them with a second slide, leaving a 100 µm gap and creating a Hele-Shaw type cell.[9] Droplet flattening makes the two reagent solutions get in contact, thus triggering the reaction, and at the same time allows a clear monitoring of the precipitation process under the microscope.

In the case of high resolution scanning electron microscopy (HRSEM) and transmission electron microscopy (TEM) imaging characterizations of precipitates, analogous experiments were carried out by putting the two reagent droplets in contact, respectively over a 0.2 µm pore filter and a carbon coated TEM grid, both supported under vacuum to quickly remove reagents solution and quench the reaction.

Small angle X-Ray scattering experiments

The coupling of SAXS experiments and solution confinement was considered in an attempt to simultaneously observe precipitation events and perform particle characterization. While small volumes would allow us to locate these events in space, a two-droplet batch reaction configuration, as previously investigated in our group by Vitry and co-workers[10] was dismissed for the SAXS experiments. Indeed, as described later on, the phase transition observed at the mixing front between the reagent solutions is extremely rapid compared to the long integration and waiting times required for data acquisition. Instead, a continuous flow mixing configuration in a microfluidic channel was preferred, thus enabling the monitoring of different reaction times as a function of channel length. For this purpose, a hybrid microfluidic platform was specifically fabricated using OSTEMER (Mercenelabs, Sweden) and Kapton 25 µm thick windows (DuPont, France), to minimize X-ray background noise and increase the detection sensitivity. Briefly, OSTEMER,[11] based on thiol-ene click chemistry,[12] is an off-stoichiometry thiol-alkene-epoxy polymer with 2 different curing steps. In a first step, OSTEMER formulation in liquid state is poured on a PDMS mould (fabricated with a low cost soft-lithographic procedure described elsewhere[13]), and subsequently placed against a first Kapton film. OSTEMER is UV cured, becoming solid, but flexible and yet sticky, so the structure can be casted from the PDMS mould. Finally a second Kapton film is added on top, and auto-glued to the OSTEMER material thanks to the remaining free epoxy groups. A final temperature curing step, completes the fabrication of the structures. The platform, (depicted below in Fig. 3a), consists on 3 different inlet channels which merge in a straight 5 cm channel with a cross section of 300x300 µm.

SAXS experiments were performed at SOLEIL synchrotron line SWING. SAXS data were acquired along the 5 cm microfluidic channel from the merging region, with a distance of 250 µm between each interrogation area. The beam size was 80x150µm². Experiments were performed using an integration time of 200 ms, with a minimum time-step time of 1000 ms between each measurement. This time-step was experimentally determined to avoid sample heating effect due to the highly energetic nature of X-Ray beam. The operation of the microfluidic platform is also schematized below in Fig. 3c. $Ce(NO_3)_3$ (0.05 m in HNO_3 1 m) and $C_2H_2O_4$ (0.075 m) solutions were injected through the side channels 1 and 3, while pure water was injected in the middle channel 2, generating a large buffering gap between the reagents. In this way, their direct contact, certainly leading to their instantaneous precipitation, is avoided. Concentrations and flow rates were optimized to avoid channel clogging while obtaining a minimum precipitate concentration ensuring a sufficient scattering signal. The diffusion of both reagents through the buffering layer of DIW leads to a precipitation region where the fluid flows merge and combine at a sufficient concentration to reach supersaturation (in green in Fig. 3c). Finally, the flow rates of reagent solutions were optimized and maintained at 1.5 $\mu L \cdot min^{-1}$, while DIW was injected with a flow rate of 40 $\mu L \cdot min^{-1}$. Bearing this in mind, the main microfluidic channel was aligned with the SAXS beam (Fig. 3b) and experiments were performed at different reaction times with a typical residence time increment, Δt, of around 33.5 ms between two consecutive interrogation areas.

Results and discussion

In the case of systems with very fast precipitation kinetics, like the one here under investigation, the mixing of reagents and the interfacial energies of reagent solutions (affecting mixing efficiency) play a major role on supersaturation generation, and therefore on precipitation. In a typical industrial application, the stirring rate is considered as the main key parameter involved in reactants mixing and homogenization even though in the case of a highly reactive media, the micromixing dynamics can have strong repercussions on nucleation pathways. When scaling down the system, *e.g.* as in the configuration considered here within droplets or in a microchannel, the convective forces are eluded by the small scale, and diffusion becomes the major contributor to solution homogenisation. Thus, the study and the understanding of the role of transport phenomena in the precipitation process is facilitated. Hence, in our first setup, the droplets of the two reagents are deposited on top of the Hele-Shaw type cell, and subsequently droplets are flattened by covering them with the cell lid until a gap of 100 microns prevails, where gravity forces and thus convection can be neglected. This planar configuration additionally becomes convenient to confine under observation the events to be monitored. Figure 1 shows a time sequence of a representative precipitation experiment, where a droplet containing a solution of 0.1 m $Ce(NO_3)_3$, in 1 m HNO_3 media, is contacted with an equivalent droplet containing a $C_2H_2O_4$ solution in stoichiometric concentration. The total duration of each experiment varies from a few tens of seconds to a few minutes, depending on the initial concentration conditions. Rapidly after the droplets coalescence takes place, a suspension composed of small emulsion-like spherical-shaped and monodisperse objects (few tens of microns when spotted) appears, describing the mixing front of the reactant droplets since the very beginning (fig. 1a to 1e). These instantaneously arising objects do not show

birefringence under crossed polarizers (Fig. 1f and 1g), thus suggesting an amorphous nature. Their concentration increases during the first seconds of the reaction, and soon we observe the transformation of one of these particles with the presence of a bright birefringent spot on the image, pointing the appearance of a crystalline phase (Fig. 1f and 1g). If we take a closer look to the new-born crystals, we can observe that they induce a local depletion area when growing, while the first precipitated species concomitantly dissolves (red circle in Fig. 1g and 1h). This is characteristic of a solvent-mediated phase transition, from a more soluble to a less soluble precipitating phase. Finally, once the second and more stable phase appears, the sol completely disappears in a short period, from a few seconds to a few minutes.

These observations are consistent with a multi-stage nucleation mechanism.[14] When the direct formation of the stable phase is not possible, overall crystallization becomes a two-stage process: the formation of the stable and organized phase (second stage) is preceded by the appearance of a metastable one (first stage). Evidently, the nucleation and growth of stable crystalline cerium oxalate from the metastable precipitate makes the kinetics of formation of the first dependent on that of the second one.[15] To enable experimental observation of the presumed precursor metastable phase, the latter must have a sufficiently long lifetime. Here, the reduction of volumes exerts as well a direct effect on decreasing nucleation rates, of stochastic nature and volume dependent. This particular effect is probabilistically preventing the more stable cerium oxalate crystalline phase to rapidly nucleate, thus delaying the observed solvent-mediated phase transition, and making possible the detection and observation of the firstly precipitating metastable phase, as it has been observed in other different systems.[8] Additionally, in the setup here presented, where transport phenomena are governed by diffusion, both the nucleation and growth processes are slowed down, thus also favouring the observation of this multi-stage mechanism occurring at high supersaturations. Note that to further describe the precipitation process occurring in our particular set-up, all the phenomena involved in the generation of supersaturation, leading to phase transition, have to be considered. That comprises the effects of the mechanical forces involved in droplet flattening when closing the cell, the reagent diffusion forces from one droplet to the other, and an extra surface tension gradient, generating the so called Marangoni effect, which is likely to create a reagent solution flow in the cell gap, etc. As schematized in Fig. 1c, this generates a curved mixing front like the one observed in our precipitation scheme, and showed in Fig. 1d. In such scenario, nucleation kinetics for the first metastable precipitate are conducting precipitation to occur faster than reagents diffusion from one droplet to the other (therefore before droplets mixing and homogenization can take place). The formation of a local supersaturation maxima generated at the droplets mixing front gives rise to precipitation events at local reagent concentrations which can temporarily reach significantly higher values than the ones achieved at equilibrium after mixing the volumes of reagent solutions.[8] Further characterization was carried out on the precipitates. Figures 2a to 2c show micrographs acquired by HRSEM over precipitates obtained by performing analogous experiments on top of a 0.2 µm membrane pore filter, as described in the experimental section. A precipitate forming smooth liquid-like regions is observed, where no evidence of spherical particles or particle aggregates down to < 100 nm HRSEM resolution could be observed, no matter the initial concentration of reagents was. Additionally, these precipitates decomposed showing bubble formation under the electron beam. This transformation has also been evidenced with other materials, and it is explained by the loss of water molecules due to the applied energy. This suggests a highly hydrated composition.[8, 16]

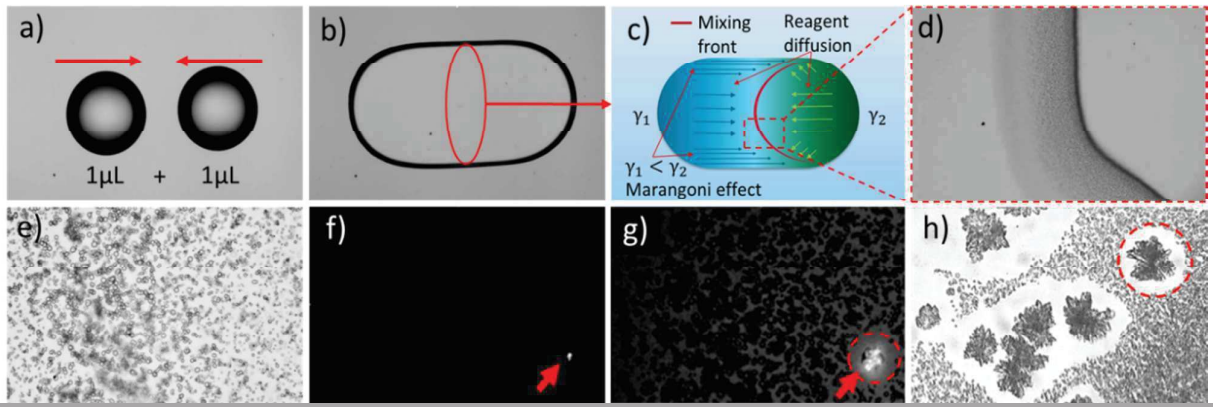

Figure 1. Time sequence of micrographs showing the course of a representative precipitation experiment. a) A 0.1 m $Ce(NO_3)_3$, in 1 m HNO_3 media, is mixed to a $C_2H_2O_4$ solution in stoichiometric concentration; b) immediately after the droplets coalescence takes place, a clear mixing front is evidenced by the instantaneous appearance of a precipitate at the droplets interface (c-d); c) sketch of the curved mixing front at the droplets interface, due to the effect of Marangoni forces close to droplets lateral free surface; d) detail of the curved mixing front depicted by the precipitation of cerium oxalate, few seconds after droplets coalescence; e) micrograph of the precipitate at higher magnification, showing droplets-like particles of a few microns size, with spherulitic and monodisperse morphology; f), g) precipitates observed under crossed polarizers showing no birefringence. Red arrows point out the appearance and growth of a cerium oxalate crystal as a

birefringent spot on the image; g), h) the new crystalline form appears and grows in the solution, by forming a local depletion area (red circles) while the first precipitate concomitantly dissolves.

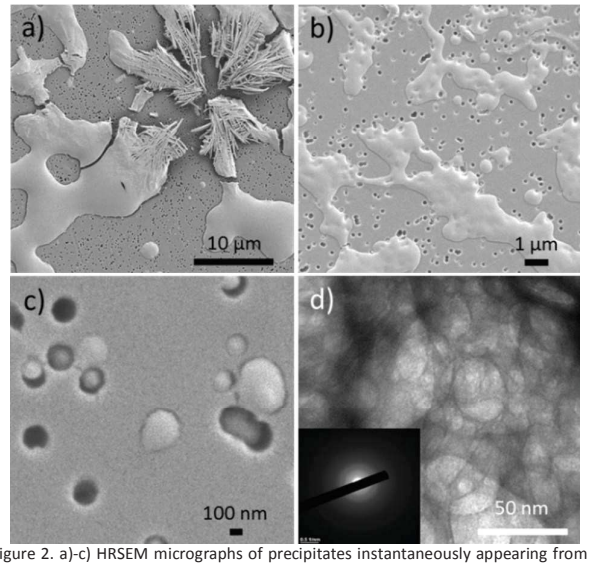

Figure 2. a)-c) HRSEM micrographs of precipitates instantaneously appearing from the coalescence of a 1 µL droplet 0.1 molar cerium nitrate in 1 molar nitric acid media, mixed to 1 µL oxalic acid solution droplet in stoichiometric concentration; d) TEM image of an analogous precipitate displaying a high porosity. Inset shows a corresponding collected SAED pattern representative from an amorphous material.

Other precipitate structures, with dendrite-like morphologies (Fig. 2a) were also observed in a lesser degree, probably due to the quick transformation of the first precipitate during sample preparation. EDX spectroscopy measurements over the crystal-like and the liquid-like structures, though not conclusive (not shown) presented different cerium/oxygen ratios, suggesting different compositions, probably due to different water contents. TEM observations (Fig. 2d) confirmed the presence of scarce sub-micron sized precipitates remaining in the carbon grid. This observed morphology can be an artifact originated by dehydration due to sample separation and TEM high vacuum conditions. Selected Area Electron Diffraction (SAED) was also conducted on the observed precipitates, which revealed amorphous as showed in inset of Fig. 2d. In this regard, and in contrast to the precipitates decomposition observed in the HRSEM characterization, electron-beam induced sample damage was not observed, probably due to the already dehydrated state of the precipitate, and thus electron-beam induced sample amorphization can be dismissed.

Bearing in mind these observations (the amorphous nature of the precipitates, and the fact that they do not retain their spherical shape during filtration and drying, proving that the cohesive energy of this amorphous particles is very low), and taking into account the low solubility of the CeOX solid phases and the high ionic activity of the reactive media, the presence of a liquid/liquid binodal, originated in the mixing fronts at local supersaturation maxima, might be taken in consideration. Accordingly, it has been recently suggested that the spinodal line is easily accessible for small molecule precipitation, within the range of supersaturations spanned by laboratory experiments.[17] In this regard, a thermodynamic modelling of the oxalate-cerium system in nitric acid aqueous media has been recently developed for a better evaluation of supersaturation conditions.[18] But a comprehensive modelling of the transport mechanisms in the experimental cell would be necessary to verify this hypothesis.

Amorphous intermediary states have already been evidenced in many crystallizing processes, including calcium oxalate precipitation.[19] However, due to their generally small size and duration, their characterization remains challenging and requires investigation tools with high spatial and temporal resolution.[20] In this context, and in order to further study the possible intervention of an amorphous state in the cerium oxalate nucleation process, preliminary SAXS experiments were performed, using an original microfluidic setup, as explained in the experimental section. In the proposed 3-channels microfluidic configuration, reagents counter-diffusion through the DIW generates at certain point supersaturation, thus triggering precipitation in a delimited region and facilitating the SAXS observations. The counter-diffusion profile is qualitatively described in Fig. 3c by the blue and yellow colours. Note that this is a simplified representation, for clarification purposes, which is not taking into account the pressure driven parabolic profile, necessarily described by the laminar flow at the microfluidic scale.[21] Figure 3d depicts the typical SAXS signals obtained at different reaction times. From all the interrogation areas explored, only the most representative scattering curves are presented, as the signal to noise ratio was too low for the other interrogation windows, probably due to the continuous change of the background signal as a function of reagent diffusion and depletion, which prevents the detection of significant SAXS signals before 0.20 s of reaction.

As a first approximation from the shape of the SAXS curves, we can infer a multimodal particles size behavior from the first spotted scattering signal. The lack of diffraction peaks is also pointing out one more time the amorphous nature of the precipitate. As the reaction time increases, particles population density increases as well, showing an intensification of the scattering signals. One possible explanation of the multimodal behavior can be found in the presumably strong reaction/transport coupling in the highly supersaturated systems. Indeed, when reagent diffusion competes with its depletion, here due to precipitation, a supersaturation wave is likely to develop across the microfluidic channel,[22] and distinct/separated precipitation events can recurrently and intermittently take place, whenever a given supersaturation threshold is crossed. This kind of behaviour, has been recently observed during CeOX precipitation under specific reagent coalescence conditions,[23] however in this study the precipitates were not characterized until droplet evaporation at the very end of the experience, and thus no metastable phase was detected. Considering that the dimensions of the X-Ray beam spot are about one half by one third of the width of the microfluidic channel, recurrent precipitation regions in the channel can be simultaneously monitored, hence explaining our observations.

Due to the limited step resolution, the background change and the tracked multimodal behavior (increasing the complexity of the scattering signal), it was not possible to analyze intermediate steps between the represented curves. However there is an interesting observation to be noted, regarding the time-evolution of the global signal. The slope of the curves obtained at the shortest reaction times (approx. -3.2, from 0.27 to 0.33 seconds of reaction) can be explained by the presence of small aggregates in fractal form at low concentrations. This explanation is consistent with a mechanism of liquid-liquid phase separation (LLPS),[24] and with our SEM mesoscale observations of an initial liquid-like precipitate. Indeed, it has been demonstrated that liquid/liquid separation may also occur for small molecules precipitation under conditions that involve the gradual increase of supersaturation, as in the setup here presented, thus pointing to a binodal rather than a spinodal route.[25] Subsequently, for reaction times larger than 0.5 seconds, from the evolution of the slope to larger values, it is possible to infer the apparition of bigger objects with a more clearly-defined surface (with a slope close to -4). Finally, at the last monitored reaction times (approx. 0.7 second) we can observe the appearance of a Guinier plateau indicating the presence of large objects of 300-400 nm, which are consistent in size and reaction times with our optical microscopy observations. Although these preliminary SAXS experiments can only be considered in qualitative terms, they provide sufficient evidence to contemplate further research on this line to corroborate the nucleation mechanisms involved in this reactive precipitation. In this regard and for a deeper comprehension of the CeOX precipitation process, future WAXS experiments are also envisaged, with a view to observe the phase transition mechanism at a molecular level.

Conclusions

An original study of the precipitation of CeOX was achieved by taking advantage of microfluidic tools and small volumes. Preliminary results are consistent with a multi-stage nucleation process, where an initially observed instantaneously precipitating, liquid-like, and amorphous highly-hydrated primary phase, subsequently undergoes a solvent-mediated phase transition to a more stable crystalline phase. Qualitative SAXS experiments are consistent with the appearance of the new phase, initially described by fractal aggregates which rapidly evolve to form larger and well-defined micron-sized particles, observable by OM during the first second of reaction. These results are opening new questions regarding the nature of this first precipitating phase and the mechanisms leading to its formation. Further experiments are required towards the full characterization of the reactive precipitation, as well as hydrodynamic modelling of the microfluidic setup in order to better assess the local and transient supersaturation conditions leading to phase transition.

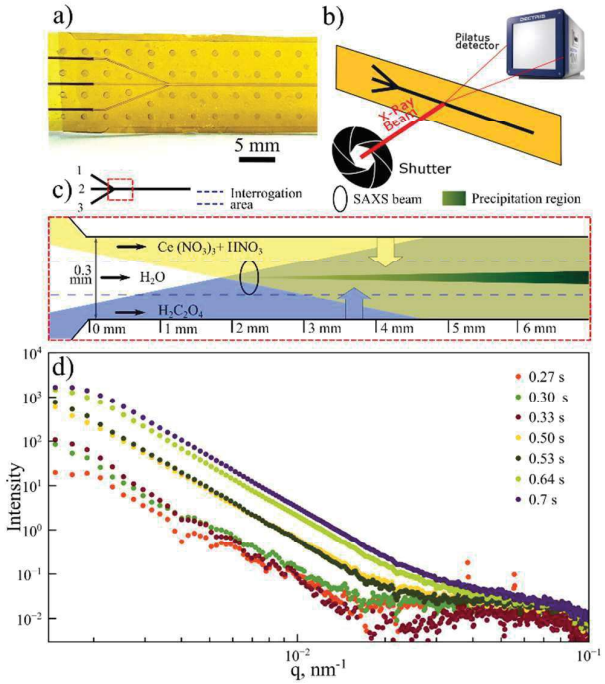

Figure 3. a) Photograph of the hybrid OSTEMER-Kapton microfluidic chip; b-c) Sketch of the microfluidic set-up used at SWING, and its operation. d) Typical SAXS curves (dots) obtained at different CeOX reaction times.

Conflicts of interest

There are no conflicts to declare.

Acknowledgements

This work was supported by the Nuclear Energy Division of CEA (DISN/PAREC). We thank SOLEIL synchrotron and Swing beam line for the provision of beam time and technological developments to support these experiments. IR-R acknowledges the CEA-Enhanced Eurotalents Program for his Incoming CEA postdoctoral fellowship.

Notes and references

1. K. Binnemans, P. T. Jones, B. Blanpain, T. Van Gerven, Y. Yang, A. Walton and M. Buchert, *Journal of Cleaner Production*, 2013, **51**, 1-22.
2. J. Torres-Arenas, J.-P. Simonin, O. Bernard, A. Ruas and P. Moisy, *Industrial & Engineering Chemistry Research*, 2010, **49**, 1937-1946.
3. J. Baldyga and W. Orciuch, *Powder Technology*, 2001, **121**, 9-19.
4. L. Vicum and M. Mazzotti, *Chemical engineering science*, 2007, **62**, 3513-3527.
5. E. Matijević and W. P. Hsu, *Journal of Colloid and Interface Science*, 1987, **118**, 506-523.
6. G. M. Pound and V. K. La Mer, *Journal of the American Chemical Society*, 1952, **74**, 2323-2332.
7. R. Grossier and S. p. Veesler, *Crystal Growth and Design*, 2009, **9**, 1917-1922.

8. I. Rodríguez-Ruiz, S. p. Veesler, J. Gómez-Morales, J. M. Delgado-López, O. Grauby, Z. Hammadi, N. Candoni and J. M. García-Ruiz, *Crystal Growth & Design*, 2014, **14**, 792-802.
9. H. S. Hele-Shaw, *Nature*, 1898, **58**, 33-36.
10. Y. Vitry, S. Teychené, S. Charton, F. Lamadie and B. Biscans, *Chemical Engineering Science*, 2015, **133**, 54-61.
11. F. Carlborg, F. Moraga, F. Saharil, W. van der Wijngaart and T. Haraldsson, 2012.
12. C. E. Hoyle and C. N. Bowman, *Angewandte Chemie International Edition*, 2010, **49**, 1540-1573.
13. I. Rodríguez-Ruiz, S. Teychené, N. Van Pham, D. Radajewski, F. Lamadie, A. Llobera and S. Charton, *Talanta*, 2017, **170**, 180-184.
14. P. G. Vekilov, *Nanoscale*, 2010, **2**, 2346-2357.
15. D. Kashchiev, *Nucleation*, Butterworth-Heinemann, 2000.
16. R. Xin, Y. Leng and N. Wang, *Journal of crystal growth*, 2006, **289**, 339-344.
17. A. F. Wallace, L. O. Hedges, A. Fernandez-Martinez, P. Raiteri, J. D. Gale, G. A. Waychunas, S. Whitelam, J. F. Banfield and J. J. De Yoreo, *Science*, 2013, **341**, 885-889.
18. I. Rodríguez-Ruiz, S. Teychené, Y. Vitry, B. Biscans and S. Charton, *Chemical Engineering Science*, 2018, **183**, 20-25.
19. E. Ruiz-Agudo, A. Burgos-Cara, C. Ruiz-Agudo, A. Ibañez-Velasco, H. Cölfen and C. Rodriguez-Navarro, *Nature communications*, 2017, **8**, 768.
20. B. Fleury, M.-A. Neouze, J.-M. Guigner, N. Menguy, O. Spalla, T. Gacoin and D. Carriere, *ACS nano*, 2014, **8**, 2602-2608.
21. P. Paul, M. Garguilo and D. Rakestraw, *Analytical Chemistry*, 1998, **70**, 2459-2467.
22. J. M. García-Ruiz, F. n. Otálora, M. L. Novella, J. A. Gavira, C. Sauter and O. Vidal, *Journal of Crystal Growth*, 2001, **232**, 149-155.
23. M. Jehannin, S. Charton, S. Karpitschka, T. Zemb, H. Möhwald and H. Riegler, *Langmuir*, 2015, **31**, 11484-11490.
24. D. Gebauer, M. Kellermeier, J. D. Gale, L. Bergström and H. Cölfen, *Chemical Society Reviews*, 2014, **43**, 2348-2371.
25. S. E. Wolf, J. Leiterer, M. Kappl, F. Emmerling and W. Tremel, *J Am Chem Soc*, 2008, **130**, 12342-12347.

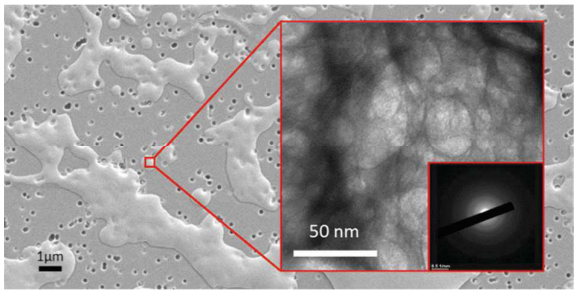

Amorphous cerium oxalate precipitates as a primary transient precursor for the crystalline phase by means of a binodal phase separation.